

Nanoscale ferroelectric tunnel junctions based on ultrathin BaTiO₃ film and Ag nanoelectrodes

X. S. Gao, J. M. Liu, K. Au, and J. Y. Dai

Citation: *Appl. Phys. Lett.* **101**, 142905 (2012); doi: 10.1063/1.4756918

View online: <http://dx.doi.org/10.1063/1.4756918>

View Table of Contents: <http://apl.aip.org/resource/1/APPLAB/v101/i14>

Published by the [American Institute of Physics](#).

Related Articles

Tuning resonant transmission through geometrical configurations of impurity clusters

J. Appl. Phys. **113**, 044305 (2013)

Electron field emission from reduced graphene oxide on polymer film

Appl. Phys. Lett. **102**, 033102 (2013)

Effect of tunneling transfer on thermal redistribution of carriers in hybrid dot-well nanostructures

J. Appl. Phys. **113**, 034309 (2013)

Negative differential resistance in electron tunneling in ultrathin films near the two-dimensional limit

J. Appl. Phys. **113**, 034308 (2013)

Simultaneous measurement of tunneling current and atomic dipole moment on Si(111)-(7×7) surface by noncontact scanning nonlinear dielectric microscopy

J. Appl. Phys. **113**, 014307 (2013)

Additional information on *Appl. Phys. Lett.*

Journal Homepage: <http://apl.aip.org/>

Journal Information: http://apl.aip.org/about/about_the_journal

Top downloads: http://apl.aip.org/features/most_downloaded

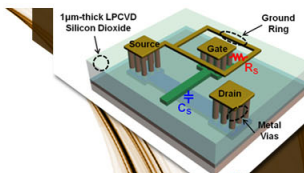
Information for Authors: <http://apl.aip.org/authors>

ADVERTISEMENT



**EXPLORE WHAT'S
NEW IN APL**

SUBMIT YOUR PAPER NOW!



SURFACES AND INTERFACES

Focusing on physical, chemical, biological, structural, optical, magnetic and electrical properties of surfaces and interfaces, and more...



ENERGY CONVERSION AND STORAGE

Focusing on all aspects of static and dynamic energy conversion, energy storage, photovoltaics, solar fuels, batteries, capacitors, thermoelectrics, and more...

Nanoscale ferroelectric tunnel junctions based on ultrathin BaTiO₃ film and Ag nanoelectrodes

X. S. Gao,^{1,2} J. M. Liu,² K. Au,¹ and J. Y. Dai^{1,a)}

¹Department of Applied Physics, The Hong Kong Polytechnic University, Hong Kong

²Institute for Advanced Materials, South China Normal University, Guangzhou, People's Republic of China

(Received 28 June 2012; accepted 17 September 2012; published online 3 October 2012)

In this work, Ag nanoisland electrodes (nanoelectrodes) have been deposited on top of ultrathin ferroelectric BaTiO₃ (BTO) films to form a nanoscale metal-ferroelectric-metal tunnel junction by integrating growth techniques of nanocluster beam source and laser-molecular beam epitaxy. The ultrathin BTO films (~ 3 nm thick) exhibit both apparent ferroelectric polarization reversal and ferroelectric tunneling related resistive switching behaviors. The introducing of Ag nanoislands (~ 20 nm in diameter) as top electrode substantially enhances the tunneling current and alters the symmetry of I - V hysteresis curves. The enhanced tunneling current is likely due to the reduction in tunneling barrier height and an increase in effective tunneling area by Ag nano-electrodes, while the improved symmetric in I - V curve may be attributed to the variation of electrode-oxide contact geometry. © 2012 American Institute of Physics. [<http://dx.doi.org/10.1063/1.4756918>]

Ferroelectric tunnel junctions (FTJs) with two metal layers sandwiched with an ultrathin ferroelectric layer as tunnel barrier have recently attracted great attention, owing to their unique electron transport properties (e.g., giant electroresistance) and application potentials in ultrahigh density recording.^{1–3} However, it is very challenging to realize such tunneling effect, which requires maintaining perfect ferroelectricity at a few nanometers scale closing to the polarization vanishing critical thickness. Until recently, thanks to the modern deposition technology, good ferroelectricity can be obtained in films as thin as a few nanometers,^{4–7} enabling the study of ferroelectric tunneling effects. Recent discoveries have demonstrated that such a nanosized tunnel junction exhibits giant electroresistivity with an *On/OFF* ratio (high resistance to low resistance) up to 2–3 orders in magnitude.^{8–13} This also enables the nondestructive resistive readout at a sub-100 nm scale, and overcomes the density limitation existing in current magnetic storage media.

The FTJ behaviors are critically depended on metal-ferroelectric interface properties, such as interface band structure, charge screening length, which can greatly affect the potential profiles and finally tunneling current.^{14–17} However, if we apply a top electrode on ultrathin films, it is very difficult to avoid the possible pinholes or defect-related leakage paths which may obscure the true current signal. Up to now, most of the FTJ studies use atomic force microscopy (AFM) tip as top electrode, which may bring about spurious effects from mechanical contact or nonuniform electrical field distribution. In a recent study, submicrometer electrodes were fabricated on top of 8 nm thick Pb(Zr,Ti)O₃ to form metal-oxide-metal (MOM) structure,¹⁸ in which a thermionic injection mechanism has been revealed. In an even thinner film (~ 2 nm) with submicrometer tunnel junction structure, FTJ tunneling behavior can be well-identified.¹⁹ These efforts pave the way for further investigating the electric

properties of ultrathin ferroelectric films using very small electrodes.

In this connection, nanometer-sized tunnel junctions based on Ag islands on top of ultrathin (1–3 nm) BaTiO₃ (BTO) films have been fabricated using an integrated system with laser molecular beam epitaxial (LMBE) and Ag nanocluster beam generator. The nanoscale tunneling junctions exhibit well-established characteristics of ferroelectric tunneling effect. More interestingly, the I - V curve symmetry can also be greatly tailored by introducing Ag nanoelectrodes.

The fabrication process of the FTJ structure is demonstrated schematically in Fig. 1. The ultrathin BaTiO₃ films were epitaxially deposited by a laser-MBE system at a temperature range of 700–750 °C and an oxygen pressure of 10 Pa. To obtain high quality BTO films, DyScO₃ (DSO) substrate was used, and SrRuO₃ (SRO) layer was deposited as bottom electrode. The Ag nanoislands of around 20 nm in diameter on top of BTO film were produced by an Ag nanocluster beam source equipped with LMBE. In brief, magnetron sputtering was used to produce Ag plasma inside a chamber filled with Ar gas atmosphere (~ 780 Pa), in which the Ag atoms collide each other and agglomerate into clusters. The clusters then eject out through a small aperture in front of the Ar chamber and from a beam of clusters. Finally, the cluster beam were deposited on top of BTO film surface and become nanoelectrodes. Ferroelectric polarization and tunneling behaviors were further characterized by piezoresponse force microscopy (PFM) and conductive AFM (C-AFM), using a commercial available Veeco multimode scanning probe microscopy (SPM). To get a better sensitivity for the PFM signals, a lock-in Amplifier (SR830 DSP) were used to pick up the weak piezoresponse signal and an ac driving amplitude (~ 0.2 V) to the bottom electrode were applied during PFM imaging, and the local piezoelectric hysteresis loops were measured in fixed locations as a function of a dc switching bias superimposed on ac driven voltage. The conductive AFM were perform with a C-AFM module, with a gain amplifier (10^9 V/A, veeco CAFM sensor), and

^{a)} Author to whom correspondence should be addressed. Electronic mail: apdaijy@inet.polyu.edu.hk.

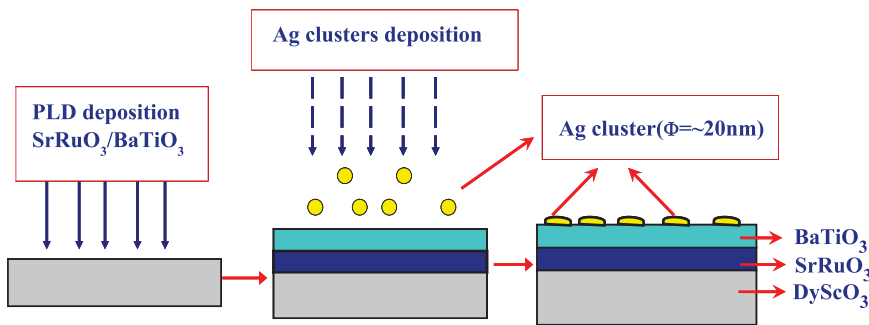


FIG. 1. Schematic diagrams of the fabrication procedure for ferroelectric tunneling junction.

the full I-V loop were also obtained by dc bias sweep at a fixing point using diamond-coated conductive probes. To further verify the existence of ferroelectricity in the ultrathin films, another scanning probe microscopy (Cypher, Asylum Research) were also employed to examine the piezoresponse amplitude and phase images, which enable domain writing using predesigned patterns. Some of SPM data were processed by using free WSxM software package.²⁰

To ensure that the BTO films grown on DyScO₃ substrate have good ferroelectricity, we first deposited 200 nm-thick BTO film as a reference. The thick BTO film shows more or less smooth surface with a remnant polarization as high as 50 $\mu\text{C}/\text{cm}^2$, comparable to that reported by Choi *et al.*²¹ To study the ferroelectric tunneling effect, ultrathin BTO film of ~ 3 nm-thick was fabricated using similar deposition parameters, as illustrated by AFM morphology and cross-sectional high resolution transmission electron microscopy (HRTEM) images (Figs. 2(a) and 2(b)). Although the film surface is not completely atomically smooth, where step terraces with a height of 2–3 atomic layers presents, it is still possible to find some atomic scale smooth areas of $500 \times 500 \text{ nm}^2$, enabling the deposition of nanometer-sized electrode on top of BTO film to form nanoscale junctions. Figs. 2(c) and 2(d) demonstrate the PFM phase and amplitude images obtained by Asylum Cypher SPM. The phase image shows well-defined bright/dark contrast regions, which are correspondent to domain patterns written by applying external bias (± 3 V) through AFM tip. The amplitude image is also shown in Fig. 2(d), in which narrow domain wall (dark lines) can be identified at the borders between the neighboring domains of opposite orientations. The polarization switching is also further examined by voltage dependent piezoresponse testing (Figs. 2(e) and 2(f)), which shows a rather square hysteresis PFM phase loop, along with a butterfly like amplitude loop, exhibiting the typical characteristics of ferroelectric polarization switching.

For memory applications, normally a real metal-ferroelectric-metal heterostructure, i.e., capacitor structure, is required. Here, we construct nanometer sized ferroelectric tunnel junction utilizing Ag nanoislands (~ 20 nm in lateral diameter) on top of the ultrathin BTO films as top electrodes. The conductivity was further characterized by C-AFM mapping, as shown in Figs. 3(a) and 3(b), where one can see that, under the same scan voltage (-1.5 V), much larger current (darker contrast) were observed in areas with Ag nanoelectrodes in contrast to the areas on bare BTO film. It is noted that most of the high current areas are located on nanodots, although there are also some dot-like regions exhibiting low

conductivity, which may be related to the occurrence of weak electrode-film contact or other nonconductive dots. The change in conductivity is further verified by the local I-V measurements shown in Figs. 3(c) and 3(d), where the current amplitude through Ag nanoelectrode can reach as high as five times of that without Ag electrode. It is also apparent that both of them show resistive switching characteristics. The *On/OFF* ratio for the high resistance state (HRS) to the low resistance state (LRS) derived from the I-V curve is in the order of 100–500 (at 1.5 V), which is in the range of reported ferroelectric tunneling.^{9,11,22} The onset voltages for the resistive switching are in the range of 1.5 V–2 V, which is rather close to the ferroelectric coercive fields as refer to Figs. 2(e) and 2(f), indicating apparent correlation between resistive switching and ferroelectric polarization reversal. The nanometer FTJ exhibits a large *ON/OFF* ratio, and is able to scale down ~ 20 nm, promising for non-destructive data storage application. It is also interesting to note that without an Ag nanoelectrode, the I-V curve exhibits more or less current rectification behavior, while the symmetry of I-V curves can be significantly improved when small Ag electrode is applied.

To further understand the mechanisms, the low voltage I-V curves were fitted by the well adopted Brinkman's direct quantum-mechanical tunneling model involving trapezoidal tunnel barriers,^{22–25} by using the equation derived by Gruverman *et al.*²⁵ For the BTO film with Ag nanoelectrode, the experimental data can fit the model fairly well (see Fig. 4(a)), and we are able to derive the interface potential barriers: $\Phi_{\text{BTO}/\text{Ag}} = 0.91$ eV and $\Phi_{\text{BTO}/\text{SRO}} = 1.15$ eV for polarization pointing up, and $\Phi_{\text{BTO}/\text{Ag}} = 1.05$ eV and $\Phi_{\text{BTO}/\text{SRO}} = 0.98$ eV for polarization pointing down. The polarization reversal can change the potential barriers with $\Delta\Phi_{\text{BTO}/\text{Ag}} = 0.14$ eV and $\Delta\Phi_{\text{BTO}/\text{SRO}} = 0.21$ eV, respectively, which can be account for by the electrostatic potential produce by the Thomas–Fermi screening induced by ferroelectric polarization.^{15,16} As a result, the changes in potential height lead to the observed resistive switching behaviors. The above fitting is comparable to other experimental reports in ferroelectric tunneling.^{20–24} It is worth of mention that at low bias voltage range (< 1 V), the current amplitude is too weak and is below the noise level, which may weaken our explanation based on ferroelectric tunneling, implying that other possible mechanisms in oxide materials may also occur. However, the rest I-V curves at moderate bias voltage range (1–1.5 V, which is below the polarization switching voltage) can fit the direct tunneling model fairly well, supporting that ferroelectric tunneling is dominating the resistive behaviors.

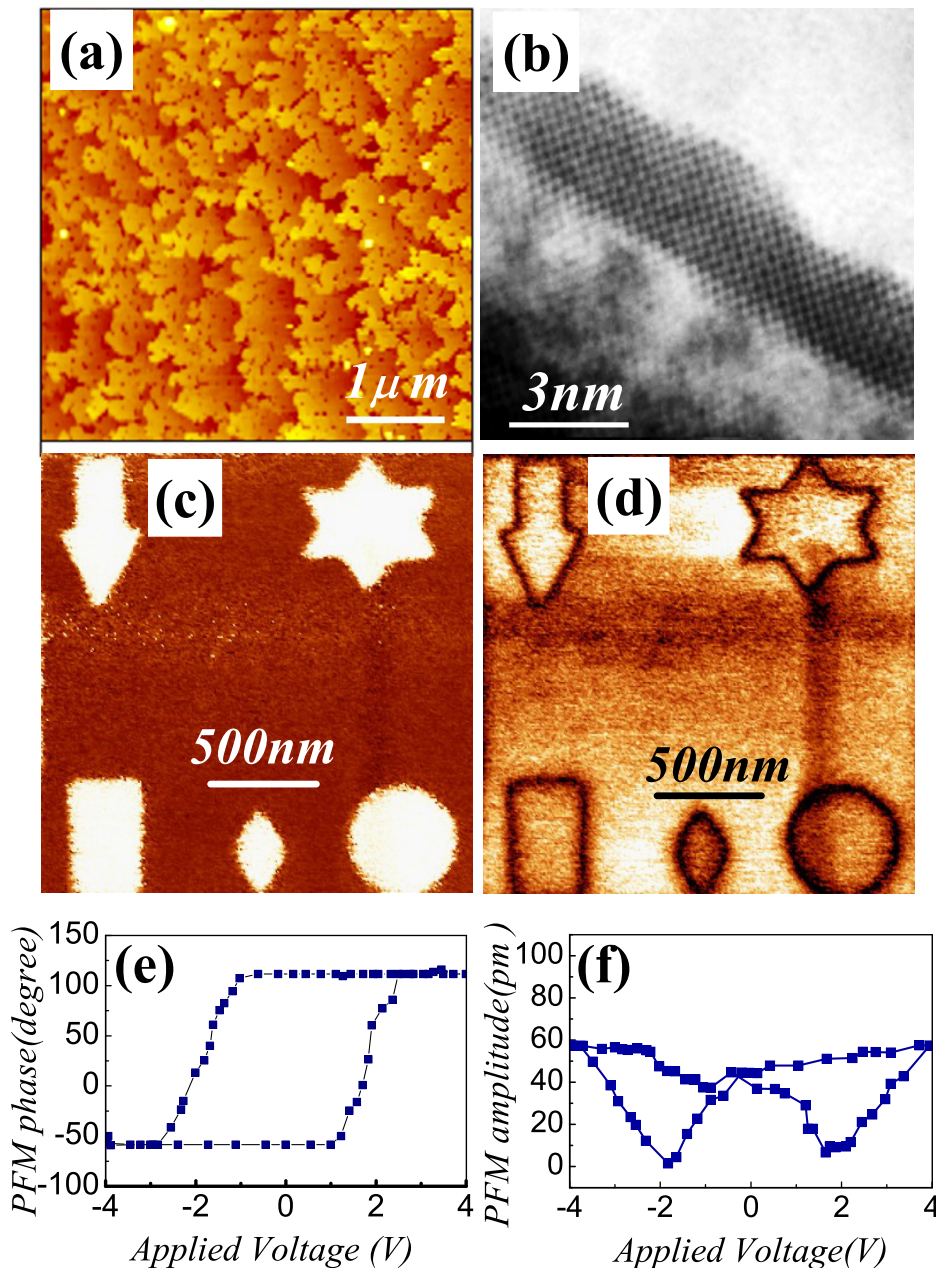


FIG. 2. AFM topological micrograph (a), HRTEM cross-sectional image (b) for the ultra-thin BTO film; piezoresponse phase (c) and amplitude (d) images, in which the bright/dark contrast were poled by applying $\pm 3\ \text{V}$ through AFM tip using a predefined pattern; voltage dependent piezoresponse amplitude (e) and phase (f) hysteresis loop for the ultrathin BTO film.

However, for the structure without Ag film, the low voltage I - V curve becomes rather asymmetric, and the fitting curve deviates a lot from the experimental data, as shown in Fig. 4(b). As mentioned previously, the conductive measurement using AFM tip may bring some spurious effects, which is rather complicated. One possible explanation for the observed current rectification can be the geometric effects from electrode-oxide contact. For the tunneling junction without Ag nanoelectrode, the tunneling only occurs at the sharp protrusion of AFM tip (e.g., upmost atoms of the tip) in spite that the contact area can be much bigger.^{16,26} The sharp protrusion generates much stronger electric field near the tip than that near the BTO/SRO interface, producing much different shapes between forward and reverse tunnel barriers, as schematically shown in Fig. 4(b). As the tunneling current greatly depends on the “area” under the tunneling barrier, the dissimilar shapes of potential barriers thus lead to the observed current rectification behavior. Similar tip

geometric effects on tunneling current rectification has been reported in a theoretic calculation in STM system.²⁵ This is more or less analogous to a MOM point contact diode, in which electrons can tunnel easily from a sharp tip to a flat metal surface, while is much difficult to tunnel backward.^{26,27} As a result, when replacing the sharp AFM tip with Ag electrodes, the point contact geometry becomes flat surface contact, hence greatly improves the symmetry of I - V curve.

It is worth to note that factors other than the direct tunneling can also affect the resistive switching behaviors in thin ferroelectric films, e.g., Fowler-Nordheim (FN) tunneling, thermionic emissions.^{23,28} At relatively higher voltage range (above the ferroelectric tunneling dominating region), the I - V curve can be well fitted to the FN tunneling equation, implying that FN plays an essential role at higher voltage range. It is also reported that thermionic emission through the Schottky barrier, may also contribute to the current

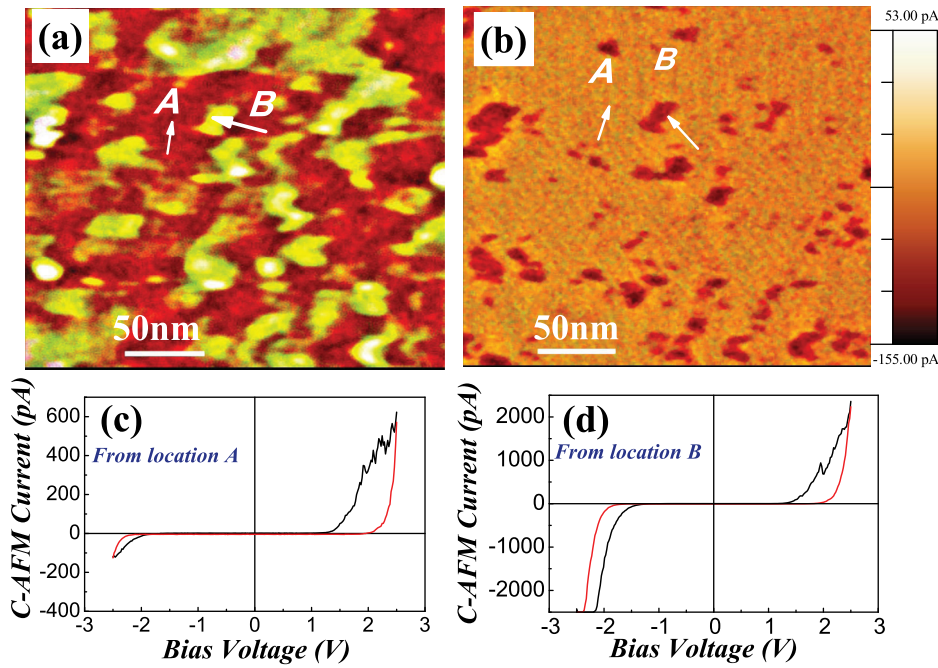


FIG. 3. Conductive-AFM measurement for the ferroelectric nanotunnel junction based on the ultrathin BTO film and nanometer-sized Ag electrodes: (a) and (b) topological and corresponding conductive-AFM mapping (scan bias of -1.5 V) for the nanotunnel junction, where the dark contrasts on Ag nanoislands indicates relatively higher conductivity. Local conductive-AFM I - V curves were measured (c) directly on BTO film surface, (d) on Ag nanoelectrode.

rectification and the large electroresistance in ferroelectric films.^{18,23} For a typical thermionic emission behavior, the I - V curve shows switchable diode-like behavior, in which the low voltage current can switch between *OFF*-state (high resistance state) to *ON*-state (low resistance state) when bias voltage changes its direction.^{23,29} In addition, polarization flip can also change the Schottky barrier, triggering another switch between *OFF* and *ON*-states. In our case, when bias voltage sweeps to opposite directions, the current states remind *ON* to *ON* (or *OFF* to *OFF*) in stead of the expected thermionic associated *On-OFF* switch. Therefore, it is unlikely that thermionic emission can play an essential role in our ultrathin films, instead the direct tunneling and FN tunneling are the dominating factors governing the conductive and electroresistive behaviors.

It is also found that the current amplitude through Ag electrode is much larger than the areas without Ag electrode under the same applied voltage. The enhancement in current amplitude can be accounted for by the enlarged effective tunneling area, which is only occurs at the sharp protrusion of AFM tip, leading to a much reduced effective tunneling area. In addition, the Ag nanoelectrode has a lower work function than that of diamond coated tip (Ag: 4.3 eV,³⁰ tungsten doped-diamond 5.12 eV³¹), which also leads to a reduction in contact barrier potential and consequently an increase in conductivity.

Finally, a metal-ferroelectric-metal tunneling junction structure with Ag nanoislands on top of ultrathin ferroelectric BTO film, have been fabricated by a system integrating a LMBE and a nanocluster beam generator. The introducing of

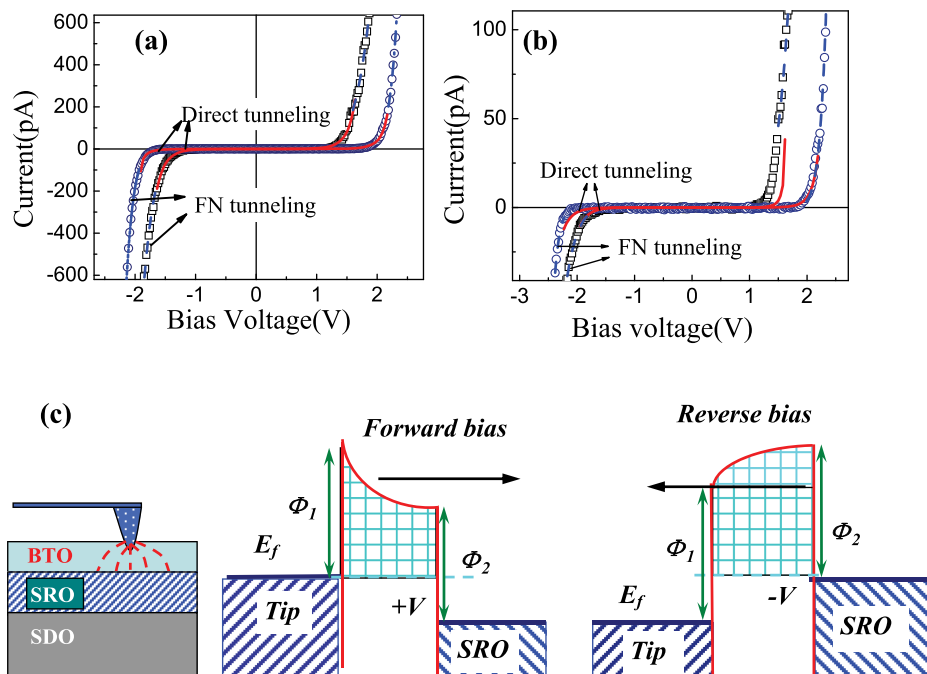


FIG. 4. Part of the experimental I - V data fitted by direct tunneling model as well as FN tunneling model for (a) BTO film with Ag nanoelectrodes, and (b) without Ag electrodes. (c) Schematically diagrams for the potential profiles of the ultrathin BTO/AFM tip tunnel junctions, which shows asymmetric shape of tunneling barriers under forward and reverse bias originating from sharp tip geometry, which may arise from nonuniform electric fields near the sharp tip.

Ag nanoislands on top of BTO film can result in apparent enhancements in both current density and symmetry in I - V hysteresis curves. The enlarged tunneling current can be ascribed to the reduction in barrier height as well as an increase in effective tunneling area by Ag electrode, while the improved current symmetry is likely due to the creation of flat electrode-oxide contact instead of point contact through the sharp protrusion of C-AFM tip.

The author J.Y.D. gratefully acknowledges the financial support from Hong Kong GRF (Grant No. 514512). The author X.S.G. also likes to acknowledge the Natural Science Foundation of China (Grant Nos. 51072061, 51031004, and 51272078) for financial assist.

- ¹L. Esaki, R. B. Laibowitz, and P. J. Stiles, *IBM Tech. Discl. Bull.* **13**, 2161 (1971).
- ²E. Y. Tsybal and H. Kohlstedt, *Science* **313**, 181 (2006).
- ³M. Dawber, K. M. Rabe, and J. F. Scott, *Rev. Mod. Phys.* **77**, 1083 (2005).
- ⁴T. Tybell, C. H. Ahn, and J.-M. Triscone, *Appl. Phys. Lett.* **75**, 856 (1999).
- ⁵D. D. Fong, G. B. Stephenson, S. K. Streiffer, J. A. Eastman, O. Auciello, P. H. Fuoss, and C. Thompson, *Science* **304**, 1650 (2004).
- ⁶J. Junquera and Ph. Ghosez, *Nature* **422**, 506 (2003).
- ⁷A. V. Bune, V. M. Fridkin, S. Ducharme, L. M. Blinov, S. P. Palto, A. Sorokin, S. G. Yudi, and A. Zlatkin, *Nature (London)* **391**, 874 (1998).
- ⁸J. Rodriguez Contreras, H. Kohlstedt, U. Poppe, R. Waser, C. Buchal, and N. A. Pertsev, *Appl. Phys. Lett.* **83**, 4595 (2003).
- ⁹V. Garcia, S. Fusil, K. Bouzehouane, S. Enouz-Vedrenne, N. D. Mathur, A. Barthélémy, and M. Bibes, *Nature* **460**, 81 (2009).
- ¹⁰M. Hambe, A. Petraru, N. A. Pertsev, P. Munroe, V. Nagarajan, and H. Kohlstedt, *Adv. Funct. Mater.* **20**, 2436 (2010).
- ¹¹A. Crassous, V. Garcia, K. Bouzehouane, S. Fusil, A. H. G. Vlooswijk, G. Rispens, B. Noheda, M. Bibes, and A. Barthélémy, *Appl. Phys. Lett.* **96**, 042901 (2010).
- ¹²M. Gajek, M. Bibes, S. Fusil, K. Bouzehouane, J. Fontcuberta, A. E. Barthelemy, and A. Fert, *Nature Mater.* **6**, 296 (2007).
- ¹³V. Garcia, M. Bibes, L. Bocher, S. Valencia, F. Kronast, A. Crassous, X. Moya, S. Enouz-Vedrenne, A. Gloter, D. Imhoff, C. Deranlot, N. D. Mathur, S. Fusil, K. Bouzehouane, and A. Barthélémy, *Science* **327**, 1106 (2010).
- ¹⁴H. Kohlstedt, N. A. Pertsev, J. Rodriguez Contreras, and R. Waser, *Phys. Rev. B* **72**, 125341 (2005).
- ¹⁵M. Y. Zhuravlev, R. F. Sabirianov, S. S. Jaswal, and E. Y. Tsybal, *Phys. Rev. Lett.* **94**, 246802 (2005).
- ¹⁶J. P. Velev, C.-G. Duan, J. D. Burton, A. Smogunov, M. K. Niranjan, E. Tosatti, S. S. Jaswal, and E. Y. Tsybal, *Nano Lett.* **9**, 427 (2009).
- ¹⁷X. Luo, B. Wang, and Y. Zheng, *ACS Nano* **5**, 1649 (2011).
- ¹⁸D. Pantel, S. Goetze, D. Hesse, and M. Alexe, *ACS Nano* **5**, 6032 (2011).
- ¹⁹D. Pantel, H. D. Lu, S. Goetze, P. Werner, D. J. Kim, A. Gruverman, D. Hesse, and M. Alexe, *Appl. Phys. Lett.* **100**, 232902 (2012).
- ²⁰I. Horcas, R. Fernandez, J. M. Gomez-Rodriguez, J. Colchero, J. Gomez-Herrero, and A. M. Baro, *Rev. Sci. Instrum.* **78**, 013705 (2007).
- ²¹K. J. Choi, M. Biegalski, Y. L. Li, A. Sharan, J. Schubert, R. Uecker, P. Reiche, Y. B. Chen, X. Q. Pan, V. Gopalan, L.-Q. Chen, D. G. Schlom, and C. B. Eom, *Science* **306**, 1005 (2004).
- ²²W. F. Brinkman, R. C. Dynes, and J. M. Rowell, *J. Appl. Phys.* **41**, 1915 (1970).
- ²³D. Pantel and M. Alexe, *Phys. Rev. B* **82**, 134105 (2010).
- ²⁴A. Chanthbouala, A. Crassous, V. Garcia, K. Bouzehouane, S. Fusil, X. Moya, J. Allibe, B. Dlubak, J. Grollier, S. Xavier, C. Deranlot, A. Moshar, R. Proksch, N. D. Mathur, M. Bibes, and A. Barthélémy, *Nat. Nanotechnol.* **7**, 101 (2012).
- ²⁵A. Gruverman, D. Wu, H. Lu, Y. Wang, H. W. Jang, C. M. Folkman, M. Y. Zhuravlev, D. Felker, M. Rzechowski, C.-B. Eom, and E. Y. Tsybal, *Nano Lett.* **9**, 3539 (2009).
- ²⁶H. Q. Nguyen, P. H. Cutler, T. E. Feuchtwang, Z.-H. Huang, Y. Kuk, P. J. Silverman, A. A. Lucas, and T. E. Sullivan, *IEEE Trans. Electron Devices* **36**, 2671 (1989).
- ²⁷D. J. E. Knight and P. T. Woods, *J. Phys. E* **9**, 898 (1976).
- ²⁸P. Maksymovych, S. Jesse, P. Yu, R. Ramesh, A. P. Baddorf, and S. V. Kalinin, *Science* **324**, 1421 (2009).
- ²⁹C. Wang, K. J. Jin, Z.-T. Xu, L. Wang, C. Ge, H.-B. Lu, H.-Z. Guo, M. He, and G.-Z. Yang, *Appl. Phys. Lett.* **98**, 192901 (2011).
- ³⁰T. Schulmeyer, S. A. Paniagua, P. A. Veneman, S. C. Jones, P. J. Hotchkiss, A. Mudalige, J. E. Pemberton, S. R. Marder, and N. R. Armstrong, *J. Mater. Chem.* **17**, 4563 (2007); H. B. Michaelson, *J. Appl. Phys.* **48**, 4729 (1977).
- ³¹K. Liu, B. Zhang, M. F. Wan, J. H. Chu, C. Johnston, and S. Roth, *Appl. Phys. Lett.* **70**, 2891 (1997).